

# iP & OEIP – Cytokinin Micro Application Modulates Root Development with High Spatial Resolution

Barbora Pařízková,\* Ioanna Antoniadou, David J. Poxson, Michal Karady, Daniel T. Simon, Marek Zatloukal, Miroslav Strnad, Karel Doležal, Ondřej Novák, and Karin Ljung\*

State-of-the-art technology based on organic electronics can be used as a flow-free delivery method for organic substances with high spatial resolution. Such highly targeted drug micro applications can be used in plant research for the regulation of physiological processes on tissue and cellular levels. Here, for the first time, an organic electronic ion pump (OEIP) is reported that can transport an isoprenoid-type cytokinin, *N*<sup>6</sup>-isopentenyladenine (iP), to intact plants. Cytokinins (CKs) are plant hormones involved in many essential physiological processes, including primary root (PR) and lateral root (LR) development. Using the *Arabidopsis thaliana* root as a model system, efficient iP delivery is demonstrated with a biological output – cytokinin-related PR and LR growth inhibition. The spatial resolution of iP delivery, defined for the first time for an organic compound, is shown to be less than 1 mm, exclusively affecting the OEIP-targeted LR. Results from the application of the high-resolution OEIP treatment method confirm previously published findings showing that the influence of CKs may vary at different stages of LR development. Thus, OEIP-based technologies offer a novel, electronically controlled method for phytohormone delivery that could contribute to unraveling cytokinin functions during different developmental processes with high specificity.

which potentially allows electronic control of their local concentrations by precise hormone delivery. Organic electronic ion pumps (OEIPs) are a novel technology that enables the highly controlled transport of various organic substances with unprecedented spatial and temporal resolution.<sup>[1]</sup> Ions are transported from a pump reservoir to a target matrix through a delivery channel carrying ion (cation/anion) exchange membranes (IEMs) with a high density of fixed charged groups. Flow-free and highly selective transport of the ions is achieved by the application of a controlled electric current, resulting in a steep concentration gradient at the delivery channel outlet. In addition, simple manipulation of the electrical parameters (voltage/current) can precisely fine-tune the amounts of molecules delivered to the target tissue.<sup>[1]</sup> The OEIP approach was primarily developed for biomedical applications for precise delivery of small neurosignaling inorganic ions, such as K<sup>+</sup>, Na<sup>+</sup>, Cl<sup>−</sup>, and


## 1. Introduction

Plant growth and development are regulated by the precise and dynamic cooperation of signaling molecules, such as plant hormones. In a cellular environment, phytohormones predominantly take the form of ions or molecules with a partial charge,

Ca<sup>2+</sup>,<sup>[2]</sup> and smaller organic compounds, such as  $\gamma$ -aminobutyric acid (GABA),<sup>[3,4]</sup> glutamate (Glu)<sup>[3]</sup> and acetylcholine (ACh).<sup>[5–7]</sup> Further optimization of IEM materials has resulted in the development of hyperbranched membranes (dendrolytes) enabling the transport of larger aromatic substances, such as the plant hormones indole-3-acetic acid (IAA)<sup>[8]</sup> or abscisic acid (ABA).<sup>[9]</sup>

B. Pařízková, M. Karady, M. Strnad, K. Doležal, O. Novák  
Laboratory of Growth Regulators  
Faculty of Science  
Palacký University and Institute of Experimental Botany  
The Czech Academy of Sciences  
Šlechtitelů 27, Olomouc CZ-78371, Czech Republic  
E-mail: barbora.parizkova@slu.se

B. Pařízková, I. Antoniadou, O. Novák, K. Ljung  
Umeå Plant Science Centre  
Department of Forest Genetics and Plant Physiology  
Swedish University of Agricultural Sciences  
901 83 Umeå, Sweden  
E-mail: karin.ljung@slu.se  
D. J. Poxson, D. T. Simon  
Laboratory of Organic Electronics  
Department of Science and Technology  
Linköping University  
60174 Norrköping, Sweden  
M. Zatloukal, K. Doležal  
Department of Chemical Biology  
Faculty of Science  
Palacký University  
Šlechtitelů 27, Olomouc CZ-78371, Czech Republic

 The ORCID identification number(s) for the author(s) of this article can be found under <https://doi.org/10.1002/admt.202101664>.

© 2022 The Authors. Advanced Materials Technologies published by Wiley-VCH GmbH. This is an open access article under the terms of the Creative Commons Attribution-NonCommercial-NoDerivs License, which permits use and distribution in any medium, provided the original work is properly cited, the use is non-commercial and no modifications or adaptations are made.

DOI: 10.1002/admt.202101664

In-plant physiology research, chemical biology approaches are fundamental in the investigation of phytohormone functions during plant development.<sup>[10]</sup> Various techniques are used for exogenous application of hormone molecules and other small synthetic compounds, such as spraying/immersion in liquid media, growing plants on agarose plates or in soil, and sophisticated microfluidic systems. However, such methods lack spatial and temporal resolution of the treatment and do not allow the dynamic control of compounds or liquid solvent delivery. In addition to chemical biology approaches, genetic manipulation can be complementarily carried out to influence endogenous hormonal concentrations via tissue- or developmental-specific up- or down-regulation of hormone biosynthetic or degradation enzymes, respectively. However, the generation of such transgenic lines is time-consuming and genetic transformation is highly challenging in many plant species. Also, constitutive genetic changes often result in alteration of the whole plant development. OEIPs overcome the challenges of standard treatment and genetic methods because they provide a flow-free and easily tunable technique for hormone delivery with dynamic electronic control of the applied hormone concentrations, enabling modulation of the development of any plant species at any developmental stage. OEIP-based systems have been shown to achieve a temporal resolution of delivery of <50 ms,<sup>[6]</sup> with the capacity to improve delivery speeds up to 10 ms and system turn-on/turn-off ratios of  $10^{10}$ .<sup>[11]</sup> Moreover, the miniaturization of OEIP geometric parameters, to generate capillary-based OEIP (c-OEIP) devices with a 20  $\mu\text{m}$  diameter OEIP delivery channel,<sup>[12]</sup> could enable treatment with single-cell resolution.

Cytokinins (CKs) are plant hormones that play a crucial role in almost all aspects of plant development, from cell division and differentiation, shoot and root morphogenesis, to regulation of leaf senescence and plant responses to environmental stimuli.<sup>[13,14]</sup> By controlling the balance between cell proliferation, elongation, and differentiation rates, CKs regulate plant growth and the generation of new organs, such as lateral roots (LRs)<sup>[15]</sup>. CKs have been shown to have an inhibitory effect in LR formation, which is critical in the earliest stages of this developmental process.<sup>[16]</sup> Significantly, CKs regulate the root system architecture (RSA) in concert with another key group of plant hormones, auxins, which, in contrast to CKs, promote LR formation.<sup>[15,17]</sup> Research on the molecular mechanisms involved in the complex crosstalk between auxins and CKs controlling root development has revealed their interaction at several different levels (biosynthesis, perception, signaling, and transport).<sup>[16,18]</sup>

CKs are derivatives of adenine substituted with an isoprenoid or aromatic side chain at the *N* position, with isoprenoid *N*<sup>6</sup>-isopentenyladenine (iP) being one of the most bioactive CK molecules.<sup>[13]</sup> Intracellular levels of the bioactive CK molecules, the CK bases, are modulated by precise regulation of CK biosynthesis and metabolic inactivation. To reduce the concentration of active forms, CK bases are typically glycosylated, predominantly to respective CK *O*-, *N*7-, and *N*9-CK glucosides, conjugated with ribose to *N*9-ribosides, phosphoribosylated to CK ribotides, or irreversibly degraded by CK dehydrogenases (CKXs).<sup>[13]</sup> CKs are signaling molecules perceived by plasma membrane-localized and endoplasmic reticulum-localized

hybrid histidine kinase (AHKs) receptors.<sup>[19]</sup> CK perception triggers a multistep phosphorylation cascade, resulting in activation of B-type Arabidopsis response regulator (ARR-Bs) transcription factors and consequent expression of CK-responsive genes.<sup>[19]</sup> Coupling of the synthetic CK-inducible Two-Component signaling Sensor (TCS) promoter with a green fluorescent protein (GFP) generates a TCSn::GFP reporter line that is commonly used to monitor global CK responses in vivo as a green fluorescent read-out.<sup>[20]</sup>

In order to gain a deeper understanding of how plant development is regulated, it is important to understand dynamic physiological processes at both the tissue and cellular level. Therefore, there is increasing demand for the development of miniaturization techniques that allow the highly targeted delivery of chemical substances. Here, we present the c-OEIP delivery method, which, for the first time, was optimized for transport of the plant hormone iP in vivo to intact seedlings of the model plant species *Arabidopsis thaliana*. To monitor changes in hormonal distribution as a response to the iP treatment, a unique double reporter line of *Arabidopsis* was generated, allowing the simultaneous visualization of both auxin and CKs *in planta*. Using the double reporter line, we showed that OEIP-delivered iP was taken up and metabolized in *Arabidopsis* roots and successfully induced changes in CK and auxin molecular and physiological responses. In addition, the spatial resolution of the transport was defined for iP, the first nucleobase substance delivered by OEIP. Precisely regulated iP treatments led to developmental changes in the RSA, including inhibition of PRs and LR. Thus, OEIP represents a novel tool for highly effective in vivo CK treatment at an unprecedented spatial resolution.

## 2. Results and Discussion

### 2.1. Optimizing Parameters for iP Delivery In Vitro

To regulate plant growth by OEIP-delivered iP efficiently, the experimental design and parameters for iP transport were initially optimized in vitro (**Figure 1**). As a general setup, a pump loaded with iP solution in the reservoir was submerged into 100  $\mu\text{L}$  of the target solution,  $\frac{1}{2}$  MS medium. Electrodes made from the conducting polymer poly(3,4-ethylenedioxythiophene) polystyrene sulfonate (PEDOT: PSS) on a poly-ethylene terephthalate (PET) substrate were immersed in both the reservoir and target solution to apply an electric field, as previously described by Poxson et al.<sup>[8]</sup> The positive electrode was always placed in the reservoir iP solution and the negative electrode was placed in the target medium (**Figure 1a**). It is important to note that in this experimental setup, the role of the distance between the OEIP tip and target tissue was not reflected. In in vivo applications (**Figure 2**), the physical parameters of the delivered compound and target matrix, which affect the diffusion coefficient depending on the hydration state of the compound in the media, significantly influence the efficiency of the delivery process. To achieve the best iP delivery efficiency, the parameters a) OEIP type, b) working concentrations of iP solution, and c) constant electrical current (**Figure 1b**) were tested by delivering iP into the liquid medium. Liquid chromatography coupled to

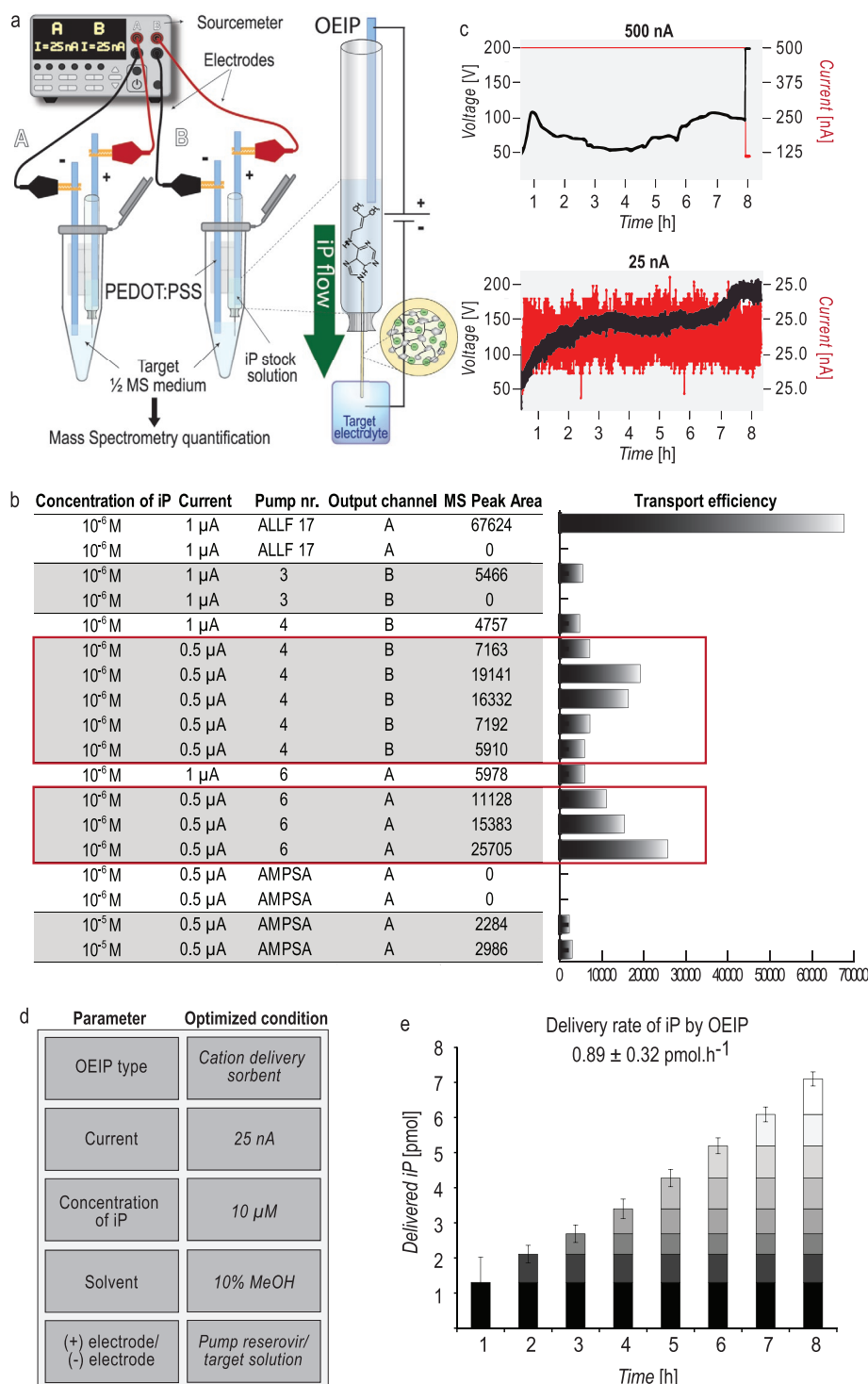


**Figure 1.** Optimization of iP delivery conditions in vitro. a) Schematic of the experimental setup for iP delivery by an OEIP into microtubes followed by relative iP quantification using LC-MS and arrangement of an OEIP device carrying a negatively charged sorbent to transport iP after electric field application. b) Optimal delivery conditions were selected based on MS detection of iP in the target medium shown in a) after 2.5 h of transport. Experimental settings providing the highest MS peak areas of iP detected in the target medium (considered as the highest transport efficiency) that were reproducible between technical replicates were selected as optimal transport conditions (red rectangles). White and gray rows represent technical replicates applying the same delivery conditions. c) Representative record of operational electrical parameters during iP delivery. Additional optimization of supplied current resulted in lower and more stable voltage supply during iP transport. d) Summary of optimized experimental conditions for OEIP delivery of iP. e) The average delivery rate of iP by an OEIP operated at the optimized conditions listed in d) was calculated as  $0.89 \pm 0.32 \text{ pmol h}^{-1}$  using the LC-MS/MS quantification method. Values represent means  $\pm$  SD,  $n = 2$ .

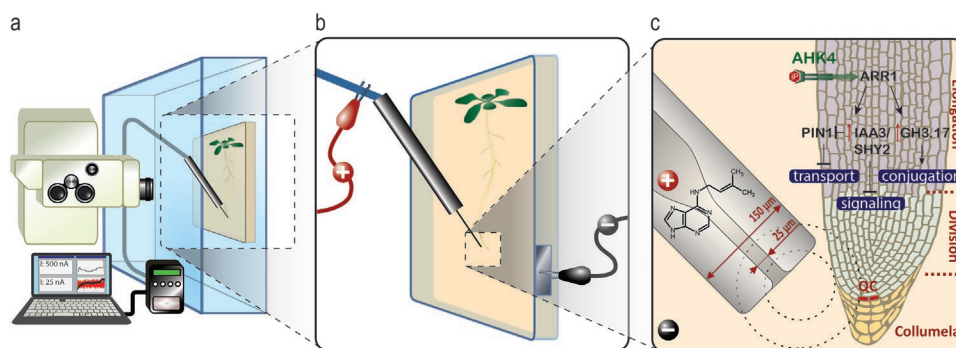


**Figure 2.** Experimental setup for high-resolution iP delivery by OEIP. a) Schematic of a vertical macroconfocal microscope with objective facing a humidifying chamber containing a vertically positioned agar plate. b) Expanded view of an agar plate with vertically grown intact *Arabidopsis* seedlings targeted with an OEIP outlet tip. c) Detailed view of an image acquired using the vertical macroconfocal microscope and OEIP outlet targeting the primary root (PR) tip of *Arabidopsis* labeled with molecular mechanisms involved in the PR CK-induced auxin response. Red spots represent auxin accumulation in the quiescent center (QC). AHK4, HYBRID HISTIDINE KINASE 4; AAR1, ARABIDOPSIS RESPONSE REGULATOR 1; PIN1, PIN-FORMED 1; SHY2/IAA3, SHORT HYPOCOTYL 2/INDOLE-3-ACETIC ACID INDUCIBLE 3; GH3.17, GRETCHEN HAGEN3.17. See also Figure S1, Supporting Information for actual images of the experimental setup.

tandem mass spectrometry (LC-MS/MS) was used to quantify the levels of iP delivered into the target medium. Based on the area of the chromatographic peaks, OEIP pumps 4 and 6, loaded with  $10^{-6}$  M iP and operated at a constant current of 0.5  $\mu$ A, provided the optimal delivery conditions, showing both the highest and most reproducible iP concentrations delivered in the target media after 2.5 h of pumping (Figure 1b). iP transported by OEIP device ALLF 17 displayed the largest MS peak area in one run but non-detectable levels of iP in another technical replicate (Figure 1b), making this device unsuitable for repeatable efficient iP delivery. However, it was previously suggested that higher operational currents can result in a great reduction of transport efficiency (ratio of the number of ions measured to leave the OEIP compared to the total electric current applied) due to the backflow of co-ions from the target to source solution.<sup>[21]</sup> To avoid this, the current was decreased from 0.5  $\mu$ A to 25 nA. Applying a current of 25 nA helped to achieve both a lower and more stable voltage supply over time (Figure 1c), as previously shown for OEIP-delivered ABA,<sup>[9]</sup> and was thus used as the optimal current for further experiments. Using the optimized delivery conditions (Figure 1d), we calculated the flow rate of iP delivery in vitro to be  $0.89 \pm 0.32$  pmol h<sup>-1</sup> (Figure 1e). Such a transport rate was significantly lower than the electric current charge equivalent rate (25 nA is equivalent to 933 pmol h<sup>-1</sup>) and lower than OEIP-delivered IAA using a different design and polyelectrolyte channel material.<sup>[8]</sup> The OEIP transport efficiency and conditions affecting the correspondence between the applied electric current and the number of transported ions is an area of an ongoing investigation that has been demonstrated to be dependent on several factors, including the OEIP device geometry, operating conditions, and charge state of the source ions.<sup>[12,21,22]</sup> The porosity of the PE membranes is also likely to be important in determining the transport efficiency but is currently poorly understood. While further investigations were not conducted in the present study, additional experiments are necessary to better understand the causes for differences in the transport efficiency of OEIPs, particularly in the case of larger and more rigid molecules. For example, adenine – the core aromatic structure of iP – can undergo

electrochemical oxidation in solution, where the extent of oxidation is strongly dependent on the electrode used.<sup>[23–25]</sup> Therefore, electrochemical oxidation of iP may represent a potential mechanism for loss of transport efficiency, where a portion of the electric current is used for oxidation instead of ion migration. Also, in a cellular environment, IAA is a weak acid with a predominant form of IAA<sup>-</sup> ions,<sup>[26]</sup> whereas iP is a molecule with a partial positive charge, making it less suitable for current-mediated transport. In addition, the higher molecular mass of iP compared to IAA may also be a factor as the size of the molecule has been shown to have a significant impact on delivery rates.<sup>[1]</sup> However, levels of CKs in plant tissues have been shown to be two orders of magnitude lower than those of IAA.<sup>[27]</sup> Indeed, cell-type-specific analyses of CKs in *Arabidopsis* root tip revealed that the concentrations of CKs ranged from 0.3 to 10 fmol per 100 000 root cells.<sup>[28]</sup> Thus, despite the lower transport efficiency of iP delivered by OEIPs, targeting only one or a few cells with a constant pmol-range delivery rate achieved using OEIP was considered to be biologically relevant and sufficient to trigger CK-related plant responses.

## 2.2. OEIP-Delivered iP Results in Tissue-Specific CK and Auxin Responses In Vivo

Next, we investigated whether the parameters optimized under in vitro conditions were suitable for iP delivery in *Arabidopsis* roots and the consequent molecular changes of CK and auxin responses in vivo (Figure 2 and Figure S1, Supporting Information). To monitor the hormonal transcriptional output, the transgenic *Arabidopsis* double reporter line *pTCSn::GFP*  $\times$  *pDR5v2::ntdTomato* was generated as a tool for sensitive and simultaneous monitoring of both CK and auxin responses after OEIP-mediated iP application. Expression of *pTCSn::GFP* is driven by a CK-responsive promoter that is upregulated in the presence of CKs.<sup>[20]</sup> Similarly, the expression of *pDR5v2::ntdTomato* red fluorescence is driven by an auxin-sensing reporter.<sup>[29]</sup> The OEIP-targeted iP supply on the PR tip significantly induced *pTCSn::GFP* expression compared to



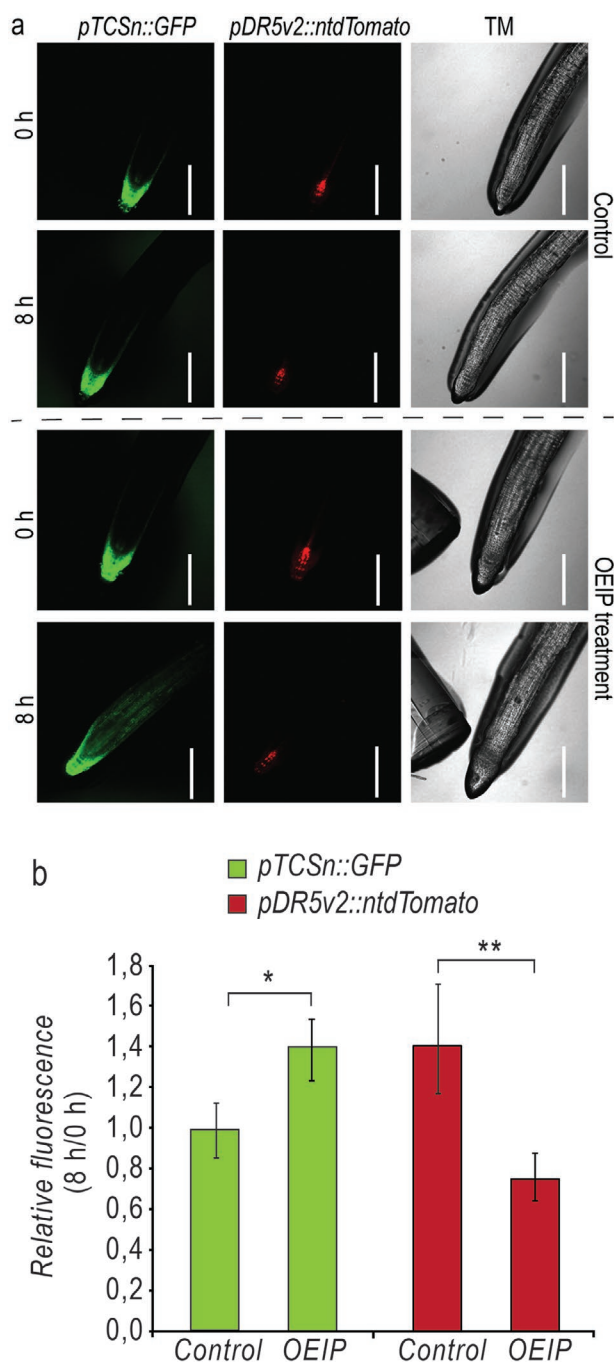


**Figure 3.** OEIP-delivered iP triggers CK-related responses in the primary root (PR). a) Representative confocal images of *Arabidopsis* seedlings displaying the cytokinin response as green fluorescence and auxin response as red fluorescence in the PR of control (non-treated) plants and iP-treated plants by OEIP at 0 h and after 8 h of treatment. Scale bar: 200  $\mu$ m. b) Relative quantification of the green and red fluorescent signals in a) expressed as corrected total cell fluorescence (CTCF). Data are presented as the ratio of signal intensities before (0 h) and after (8 h) iP treatment. Values represent means  $\pm$  SD,  $n = 4$ , one OEIP-treated root, and one control root/independent biological replicate. Statistical analysis was carried out using the two-tailed two-sided independent Student's  $t$ -test to compare iP-treated roots with non-treated controls ( $p$ -values:  $*p < 0.01$ ;  $**p < 0.001$ ). TM – transmitted light.

control roots after 8 h of iP delivery (Figure 3a,b). Importantly, the *TCSn* expression pattern, showing a significantly enhanced GFP signal in the root apical meristem and vascular tissue of the meristematic and elongation zones (Figure S2a, Supporting Information), corresponded with the fluorescent pattern observed after iP treatment by the standard immersion method in liquid medium<sup>[30]</sup> displayed by the single *pTCSn::GFP* reporter line.<sup>[20]</sup> On the other hand, the overall red fluorescent quantification revealed a reduced *pDR5v2::ntdTomato* signal in the PR tip (Figure 3a,b), as also observed after treatment with another CK representative, *N*<sup>6</sup>-benzyladenine (BA).<sup>[31]</sup> This decrease in *pDR5v2* expression was restricted to cells of the columella and quiescent center (Figure S2b, Supporting Information) where auxin response maxima are typically established as a result of local auxin biosynthesis, degradation, and auxin transport, as evidenced by various detection methods.<sup>[32]</sup> Notably, CKs were shown to reduce the auxin response by affecting all of the aforementioned molecular aspects, contributing to auxin accumulation in the root apex<sup>[33]</sup> (Figure 2c). Among others, CKs were shown to inhibit auxin signaling by activating the transcription of auxin signaling inhibitor SHORT HYPOCOTYL 2 (SHY2),<sup>[34]</sup> promoting the expression of auxin degradation enzyme GRETCHEN HAGEN3.17 (GH3.17)<sup>[35]</sup> and downregulating the expression of PIN-FORMED (PIN) auxin transporters that regulate rootward auxin transport,<sup>[31,34]</sup> all of which may have contributed to the observed reduction of auxin response. The opposite effects of iP on the CK and auxin responses in the root tip are in accordance with previously described antagonist interactions of the two phytohormones during root development.<sup>[18]</sup>

### 2.3. OEIP-Delivered iP is Taken Up and Metabolized In Vivo

To confirm that the induced *pTCSn* expression pattern was a result of efficiently delivered iP taken up by the root, we carried out LC-MS/MS quantification of iP in 1 cm root segments of OEIP-treated and control roots (Figure 4a). The analysis indicated that the observed induced CK response in OEIP-pumped root segments was caused by the elevated levels of iP and its metabolites (Figure 4b). To investigate further how OEIP-transported iP was taken up and metabolized by the plant, we performed an OEIP delivery experiment with the same experimental design (Figure 4a) using isotopically labeled [<sup>15</sup>N<sub>4</sub>-purine]iP. Such feeding experiments, using synthetic CK derivatives that do not naturally occur in nature but undergo the same metabolic conversions as native CKs, are powerful tools to investigate CK metabolism *in planta*.<sup>[36]</sup> The labeled iP and its corresponding <sup>15</sup>N<sub>4</sub>-labeled metabolites were detected in the root segments after OEIP delivery, with [<sup>15</sup>N<sub>4</sub>]-isopentenyladenine-7-glucoside ([<sup>15</sup>N<sub>4</sub>]iP7G) being the predominant species formed by [<sup>15</sup>N<sub>4</sub>]iP metabolism (Figure 4c), as previously shown in *Arabidopsis*.<sup>[37,38]</sup> The expected rapid turnover of active iP into the respective *N*-glucosides was consistent with the fact that endogenous iP levels are strictly regulated by homeostatic mechanisms; *N*-glucosylation has been shown to be the main pathway for irreversible iP inactivation.<sup>[39]</sup> Importantly, no [<sup>15</sup>N<sub>4</sub>] iP derivatives were detected in the control plants (Figure 4a).

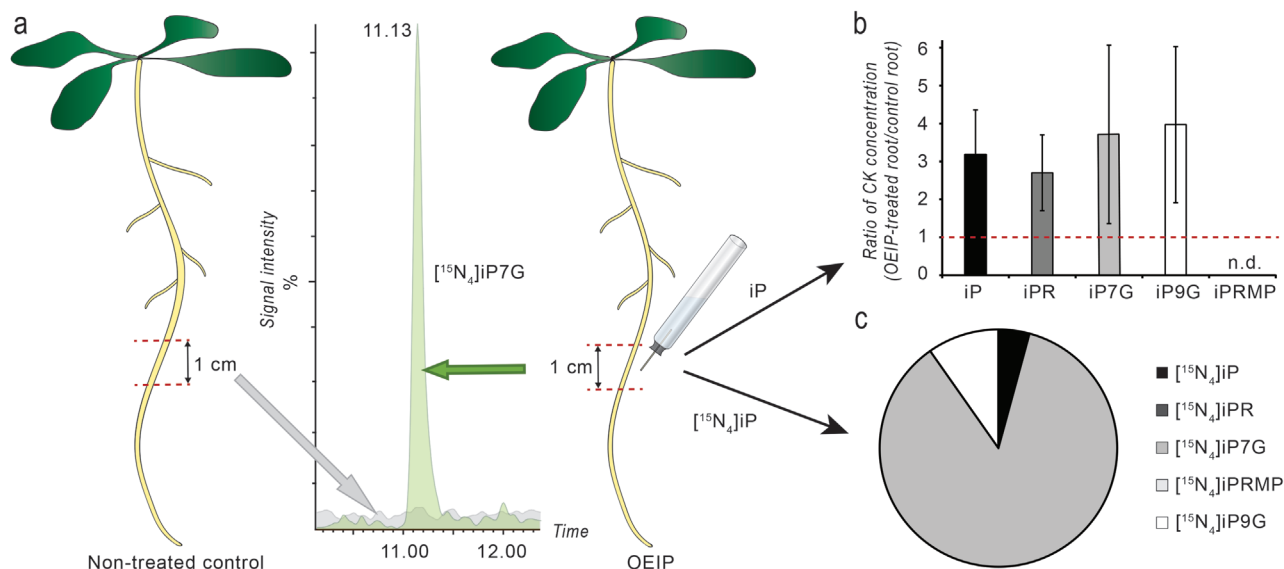


**Figure 4.** OEIP-delivered iP is taken up and metabolized *in planta*. a) Schematic of the experimental design. Intact *Arabidopsis* seedlings were treated for 24 h by OEIP-delivered iP or [ $^{15}\text{N}_4$ ]iP. The roots of OEIP-treated plants at the site of iP micro application (1 cm segments) were collected after treatment as well as non-treated control roots, and LC-MS quantification of iP/[ $^{15}\text{N}_4$ ]iP and their metabolites was carried out. LC-MS/MS chromatogram of [ $^{15}\text{N}_4$ ]iP7G (green) is shown as a representative analyte identified in OEIP treated roots, whereas no [ $^{15}\text{N}_4$ ]iP7G was detected in control roots (grey). b) Ratios of CK concentrations determined in fmol per root segment between iP-treated root segments with OEIP and non-treated control segments after 24 h treatment. Values represent means  $\pm$  SD,  $n = 3$ , one independent replicate represents five pooled root segments. c) Relative abundance of [ $^{15}\text{N}_4$ ]iP and its metabolites in [ $^{15}\text{N}_4$ ]iP-treated root segments after 24 h of treatment.

These data provided clear evidence that OEIP-delivered iP was taken up and metabolized *in vivo*, and thus potentially capable of triggering physiological responses.

## 2.4. Regulating Plant Responses with High-Resolution iP Delivery

When considering the use of OEIPs as a tool for the micro application of diverse chemical substances, delivery with high spatial resolution is regarded as a fundamental aspect.<sup>[1]</sup> The resolution is mainly governed by the radius of the concentration gradient generated at the OEIP outlet (Figure 2b and Figure S1, Supporting Information). This is highly dependent on different variables, such as the geometric parameters of the pump channel outlet, applied current/voltage,<sup>[1,21]</sup> chemical-physical properties of the delivered compound, its diffusion coefficient, and concentration of the compound in the pump reservoir solution.<sup>[8,9]</sup> All these aspects can be easily adjusted, making the OEIP-facilitated treatment method ideal for fine-tuning desired concentrations. The shape of the concentration gradients can be simulated using computational models that include the compound delivery rate, its diffusion coefficient, and transport properties in the target matrix, which can help to estimate the resolution of the delivery.<sup>[5]</sup>

After demonstrating that it was possible to transport iP into plant roots (Figure 4a,c), we aimed to determine the spatial resolution through biological relevance rather than computational modeling. Thus, the RSA of the *Arabidopsis pTCSn::GFP* expressing line was chosen as a model system. The resolution of the iP delivery was represented by *pTCSn* expression in LRs

adjacent to the OEIP-treated root as a function of distance from the OEIP (Figure 5a). Whereas the GFP signal was greatly enhanced in the root targeted by OEIP (Figure 5a,b), *pTCSn* in the neighboring LRs was not affected regardless of the distance from the pump (Figure 5a,c), confirming the high spatial resolution of OEIP delivery of less than 1 mm (Figure 5c). Although iP is known to be translocated by long-distance transport, primarily by the phloem from shoots to roots,<sup>[40]</sup> our data suggested that the long-distance transport of iP from the site of application, in the timeframe of our experiments, did not influence the CK response near to the OEIP. In addition, the relative size of the OEIP delivery channel (25  $\mu\text{m}$ ) compared to that of fully elongated root cells (up to 150  $\mu\text{m}$ )<sup>[41]</sup> means single-cell resolution for delivery is potentially achievable. We believe that OEIPs could be a convenient tool to complement genetic approaches to enable endogenous modulation of local tissue-specific hormonal levels. As shown in the following sections, OEIPs can precisely deliver plant hormones into specific tissues<sup>[8,9]</sup> at precise developmental stages, thus combining the high spatial and temporal resolution of delivery whilst elegantly overcoming some of the limitations of genetic methods.

## 2.5. Application of an OEIP Device for the Modulation of CK-Related Developmental Processes

### 2.5.1. PR Growth Inhibition

Since CKs play a central role in various developmental events, we further examined whether it was possible to modulate CK-related processes with targeted OEIP application of iP. Among

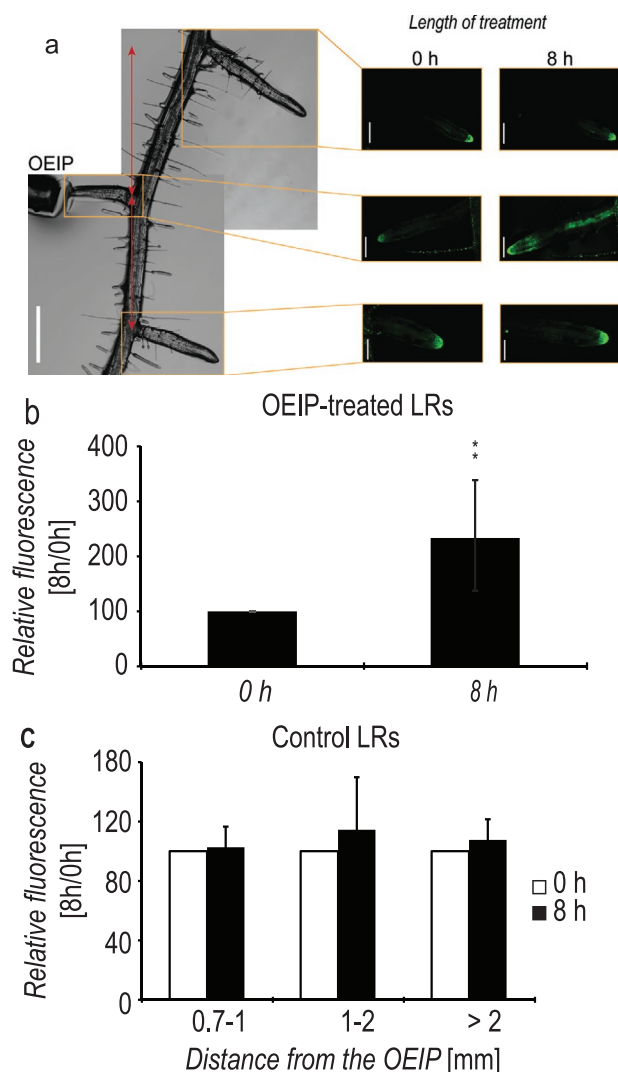


**Figure 5.** Spatial resolution of iP delivery. a) Cytokinin responses represented as a green fluorescent signal (yellow rectangles) in control non-treated (upper and bottom panel) and iP-treated (middle panel) *Arabidopsis* lateral roots (LRs) before (0 h) and after 8 h of iP treatment. Red arrows represent the distance of control LR (non-treated) from the OEIP-treated root. Scale bars represent 300  $\mu$ m in the transmitted light microscope image and 100  $\mu$ m in the confocal images. b) Relative quantification of the green fluorescent signal (in %) expressed as the ratio of fluorescent intensity before (0 h) and after (8 h) iP treatment in OEIP-targeted lateral root (LR). The signal intensity ratio at 0 h represents 100%. Values represent means of CTCF  $\pm$  SD,  $n = 7$ , every biological replicate derived from an independent experiment. Statistical analysis was carried out using the two-tailed two-sided independent Student's *t*-test to compare fluorescence intensity before (0 h) and after (8 h) iP treatment ( $p$ -value:  $***p < 0.001$ ). c) Relative quantification of the green fluorescent signal in control LR adjacent to the OEIP-treated root as a function of the root distance from the OEIP. Data are presented as the ratio of signal intensities before (0 h) and after (8 h) iP treatment of the OEIP-targeted LR. The signal intensity ratio at 0 h represents 100%. Values represent means  $\pm$  SD,  $n = 2$  (one control root above and one below the OEIP-treated root) in seven independent biological replicates. Statistical analysis was carried out using the two-tailed two-sided independent Student's *t*-test to compare the fluorescence intensity in control LR before (0 h) and after (8 h) iP treatment of the OEIP-targeted LR.

others, CKs play a crucial role in PR growth, specifically controlling root meristem size, by fine-tuning the balance between root cell proliferation, elongation, and differentiation.<sup>[18]</sup> Maintenance of the meristem relies on establishing a rate of cell division that it is equal to the rate of cells exiting the meristem and entering the differentiation-elongation zone<sup>[42]</sup> (Figure 2). Exogenous application of CKs impairs this balance, resulting in a shorter meristem and consequent retardation of PR growth.<sup>[42]</sup> To evaluate the effect of OEIP-delivered iP on the growth of the PR tip (Figure 6a), we reconstructed the root tip growth by calculating the difference in X and Y coordinates acquired using confocal microscopy software before ( $t_0$ ) and at different time-points ( $t$ ) up to 8 h of iP delivery by OEIP as  $\Delta X [X_t - X_{t_0}]$ ,  $\Delta Y [Y_t - Y_{t_0}]$ . The root tips of *Arabidopsis* seedlings targeted with OEIP-delivered iP displayed reduced growth rates compared to control roots (Figure 6b,c), in agreement with the previously shown inhibition effect of exogenous CKs on PR growth.<sup>[43–46]</sup>

### 2.5.2. Stage-Specific Inhibition of LR Development

Apart from regulating PR growth, CKs are also crucial for regulating the formation and development of LRs, thus controlling the RSA.<sup>[16]</sup> LRs undergo eight well-defined stages of development: from the first founder cells' division, LR morphogenesis, and formation of LR primordia to LR emergence from the parental root<sup>[17]</sup> (Figure 7a). In the early stages of LR initiation, CKs block the first division of LR founder cells, and thus suppress the consequent LR development.<sup>[46,47]</sup>

We investigated whether LR development could be stage-specifically modulated by OEIP-delivered iP using the *Arabidopsis* Cyclin B (CYCB) *CYCB1;1::GFP*<sup>[48]</sup> marker line. CYCB, a small protein expressed during a cell cycle to regulate cycle progression, is widely used as a marker to visualize cell division, and thus determine sites of LR initiation.<sup>[49]</sup> LR primordia targeted with OEIP-transported iP displayed a complete loss of the *CYCB1;1::GFP* signal and inhibition of LR development after overnight treatment (Figure 7b). These results were in agreement with previous findings where the expression of CYCB1 was shown to be disturbed by exogenous CK application.<sup>[46,47]</sup> Another aspect of the CK inhibitory role in LR formation is antagonization of auxin signaling by degradation of PIN proteins and redistribution of auxin from the LR initiation site.<sup>[50]</sup> CKs inhibit the transcription of PIN genes and decrease the plasma membrane PIN1-GFP signal through an AHK-based signaling machinery during LR organogenesis.<sup>[16]</sup> Downregulation of the *pDR5v2::ntdTomato* signal and inhibition of the growth of OEIP-targeted LR primordia (Figure S3, Supporting Information) additionally confirmed the efficient modulation of LR development by OEIP-delivered iP. Importantly, the LR primordia developing on the same seedling, and in close proximity to the pumped LR primordia, remained unaffected and resulted in LR emergence after 8 h (Figure 7b). These findings confirmed the precise and highly targeted regulation of LR growth in roots treated by the OEIP. It should be noted that 24% of the OEIP-treated LRs exhibited normal LR stage progression despite iP micro application (Figure S4a,b). This can be explained by a LR stage-selective inhibitory effect

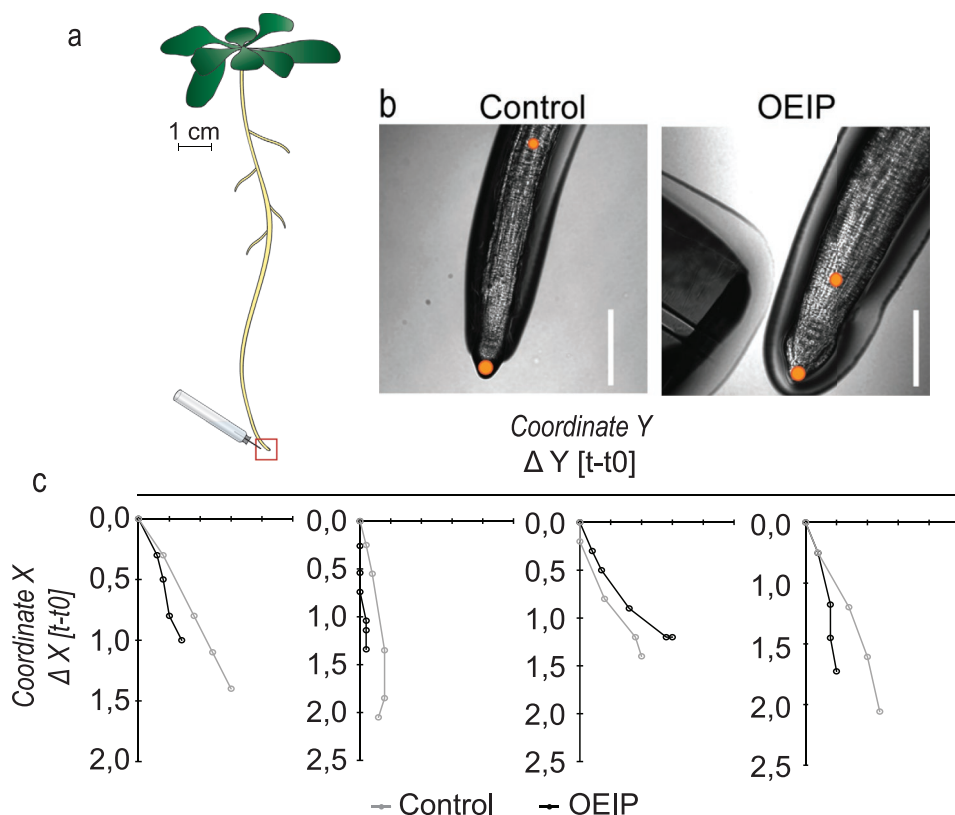


**Figure 6.** OEIP-delivered iP inhibits primary root (PR) growth. a) Schematic of *Arabidopsis* seedling showing the PR tip targeted by OEIP. The root zone assessed in b) and c) is highlighted in the red rectangle. b) Schematic light microscopy images showing iP-related inhibition of *Arabidopsis* PR growth. Orange circles indicate root positions at time 0 h and after 8 h of OEIP treatment. Scale bars represent 200 μm. c) Reconstruction of *Arabidopsis* PR growth of four roots in independent biological replicates (experiment shown in Figure 3) based on the coordinates marking the root positions at different time points during the confocal imaging. Each point of the chart represents a difference between X and Y coordinates at a particular time-point ( $t$ ) and coordinates at time 0 h ( $t_0$ ), expressed as  $\Delta X$  ( $X_t - X_{t_0}$ ) and  $\Delta Y$  ( $Y_t - Y_{t_0}$ ).

of CKs during LR, being restricted to only the early stages (I–V) of LR organogenesis (Figure S4c, Supporting Information).<sup>[51,52]</sup> Even exogenous CK application was unable to impair the development of LR primordia after stage V<sup>[51]</sup> (Figure S4a, Supporting Information). Nevertheless, the quantification of developed/inhibited roots during OEIP treatment revealed 76% and 73% of positive events (inhibition of OEIP-treated roots and standard growth of control roots, respectively, Figure S4b, Supporting Information), suggesting that modulation of LR development could be regulated by OEIP-delivered iP. Taken together, by employing OEIP we could recreate the reported LR stage-specific inhibitory effect of CKs on LR development but with a greater spatial resolution of the treatment, affecting only the targeted LR primordia.

### 3. Conclusion

In this study, we demonstrated the OEIP mediated delivery of CK iP, an important plant signaling molecule, to living plant root tissue at a spatial resolution of less than 1 mm. Using optimized conditions developed in vitro for iP delivery by OEIP, we achieved a stable and reproducible transfer rate of iP to the target tissue at biologically relevant concentrations. The results

showed the potential of OEIPs to obtain high spatial and temporal resolution for the delivery of different signaling molecules. Importantly, the intact *Arabidopsis* seedlings supplied with OEIP-delivered iP exhibited active uptake and metabolism of the delivered molecule. When applied at the root tip of the novel double reporter line *pTCSn::GFP*  $\times$  *pDR5v2::ntdTomato*, iP triggered a CK response, whereas its effect was opposite for the auxin reporter. From a physiological point of view, OEIP-delivered iP treatment led to the inhibition of both PR growth and LR stage-specific development. We showed that the developmental effects of OEIP-transported iP were in accordance with previously described roles for CKs during plant development. In addition, the novel *Arabidopsis* double reporter line, enabling the simultaneous visualization of both auxin and CK responses in vivo, could serve as a valuable tool for plant physiology research.

By combining the OEIP delivery approach with the novel *Arabidopsis* double reporter line and confocal imaging during specific developmental processes, we developed an interdisciplinary technique that utilizes the strengths of both materials science and plant biology. Our results may contribute to a better understanding and improvement of the delivery efficiency of different types of organic molecules and to the developing novel devices that enable the transport of compounds in



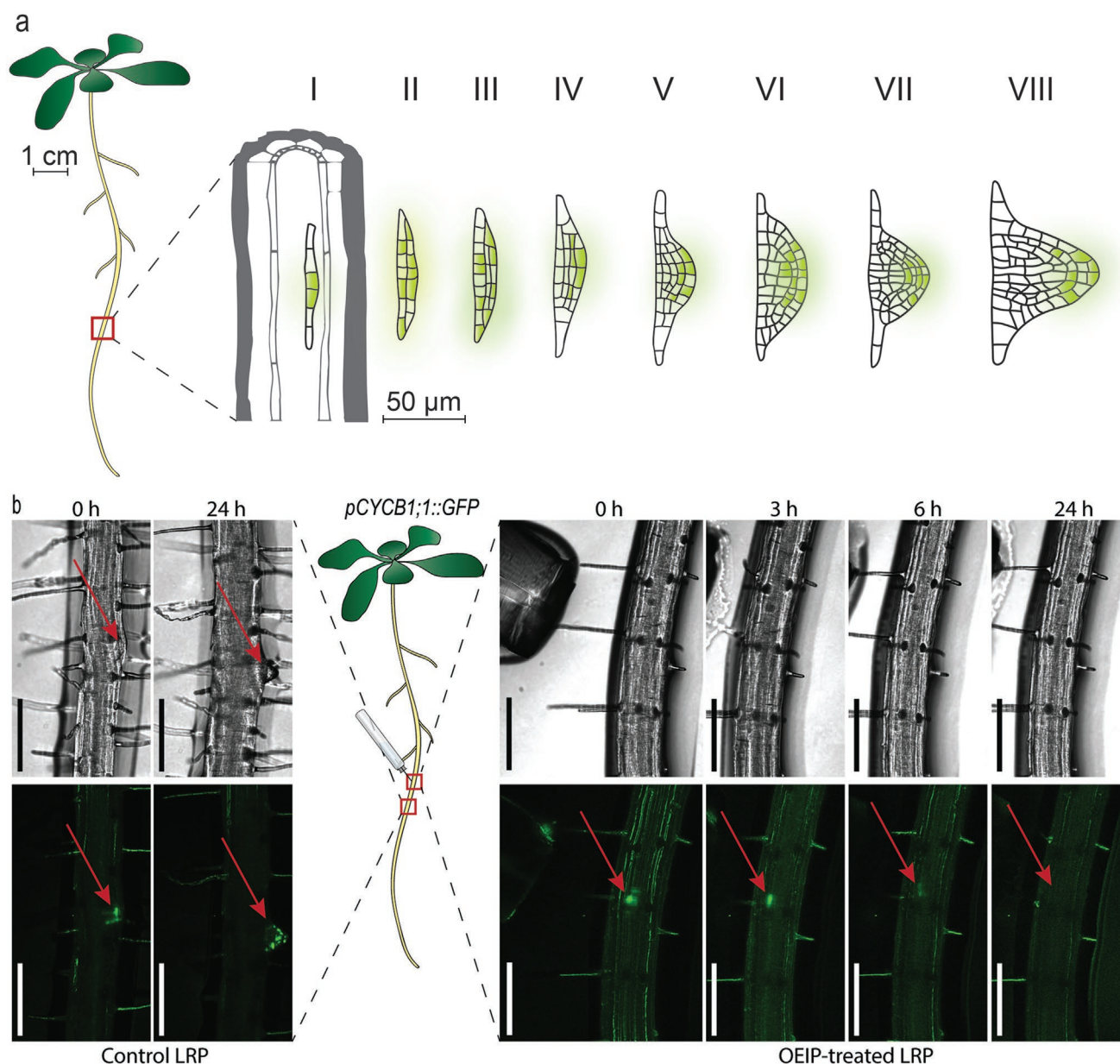


**Figure 7.** OEIP-targeted iP treatment inhibits the development of a single lateral root (LR). a) Schematic of LR development in the eight defined developmental stages. The schematic was adapted and reproduced with permission.<sup>[17]</sup> Copyright 2009, Elsevier. The red rectangle indicates the LR initiation site that is not visible to the naked eye. Green coloring indicates green fluorescent dividing cells in *pCYCB1;1::GFP Arabidopsis* seedlings, marking developing LR primordia. b) Confocal image-based real-time analysis of *pCYCB1;1::GFP* developing LR primordia in control (non-treated) and iP-treated sites of LR initiations (red arrows). The close proximity (average distance of 2.17 mm) of the control and treated LR primordia is shown by the red rectangles on the root of the *Arabidopsis* seedling scheme. Scale bars represent 200 µm.

various ambient natural matrices, such as soil. OEIPs can be used as a tool that bridges electronics and biological systems, enabling dynamic modulation of physiological processes by electronic dose control and precise delivery of various signaling molecules. This compound delivery method can overcome the drawbacks of conventional treatment techniques, namely, low spatial resolution, burst or uncontrolled compound release, and solvent delivery effects on local pressure and native ionic concentration gradients. Further, the dynamic and precise aspects of OEIP compound delivery can

complement plant genetic engineering approaches, which suffer from issues such as long generation times for construct-carrying lines, problematic transformation of some plant species or genetic modifications affecting proper plant development. Alone or in concert with other research techniques, we anticipate that with continued development, OEIP-based technology could provide a valuable and efficient tool for unraveling a wide spectrum of dynamic biological processes in any plant species with high spatiotemporal resolution at the tissue and cellular level.

## 4. Experimental Section

**Generation of Cation-Delivery OEIPs:** Silica capillaries (25/125  $\mu\text{m}$  inner/outer diameter, Molex TSP025150) were used and fabricated by a protocol previously reported.<sup>[53,54]</sup> The 12.5  $\mu\text{m}$  protective polyimide coating of the capillaries was removed by immersion in a hot bath (120 °C) of concentrated sulfuric acid, and the resulting capillaries were thoroughly rinsed in Di water. Subsequently, 20 cm sections of each capillary were cut and flushed with H<sub>2</sub>O by using dry nitrogen (5 bar). Next, the inner capillary wall was surface-treated to improve adhesion to acrylates.<sup>[55]</sup> A solution of KOH (2 M, aq) was flushed through the capillary sections for 2 h and purged using dry nitrogen for 5 min. Immediately afterward, a 10 wt% solution of 3-(trimethoxysilyl)propyl acrylate in toluene was flushed through the capillary sections for 2 h and subsequently purged with dry nitrogen for 5 min.

After surface modification, the capillary sections were filled with a solution of the polyelectrolyte (5 bar, approximately 20 min), 2-acrylamido-2-methylpropane sulfonic acid (4 mL AMPS, 50 wt% in Di), poly(ethylene glycol diacrylate) (109  $\mu\text{L}$ ; crosslinker, M.W. 700 g mol<sup>-1</sup>) and 2-hydroxy-4'-(2-hydroxyethoxy)-2-methylpropiophenone (10 mg; photoinitiator). After filling, the capillary sections were exposed to ultraviolet light (254 nm) for 10 min. Individual capillary pieces (15 mm) were cleaved with a manual fiber cleaver (Fujikura CT-02) and were immediately mounted inside an adhesive-lined plastic shrink tube (15 mm). One side of the shrink tube (4 mm) was heated with a hot air gun and a 7 mm long capillary piece was inserted into the tube. The heat tube opening was quickly clamped shut around the capillary before the glue had time to cool.

**Optimized Conditions for OEIP Storage and Operation:** When not in use, the OEIP devices were stored in 10% MeOH at 22 °C. Before each experiment, the OEIP reservoir was loaded with a fresh solution of iP (10<sup>-5</sup> M) dissolved in 10% MeOH. A positive electrode was placed in the pump reservoir containing iP stock solution, whereas a negative electrode was placed in ½ Murashige and Skoog (MS) medium: a) liquid medium in 1.5 ml microtubes with no added agar was used for method optimization and determination of delivery flow rate by LC-MS, b) solid medium covering square Petri dishes was used for confocal imaging (see particular sections below). Poly(3,4-ethylenedioxythiophene) polystyrene sulfonate (PEDOT:PSS) material on a PET substrate (cut from Orgacon F-350 film; AGFA – Gevaert) was used as an electrode extension in both the OEIP reservoir and target ½ MS medium. A Keithley 2612b SourceMeter operated with LabVIEW software (National Instruments Corp.) was used to provide the OEIP with a constant current of 25 nA.

**Plant Material and Growth Conditions:** Surface-sterilized seeds of *Arabidopsis thaliana* in Col-0 WT background were sown on 12 × 12 cm square Petri dishes with ½ MS containing MS medium (2.2 g L<sup>-1</sup>; Duchefa Biochemie, M0222), sucrose (1%), plant agar (0.7%; Duchefa), 2-(N-morpholino)ethanesulfonic acid (MES) (0.5 g L<sup>-1</sup>; Sigma Aldrich), pH 5.6 (adjusted with 1 M KOH). The seeds were stratified for 2 days in the dark at 4 °C and then transferred to a growth chamber. Seedlings were grown vertically under standard light conditions (22 °C, 16 h light/8 h dark) for 11 days. The *pCYCB1::GFP* line has been described elsewhere.<sup>[48]</sup>

**Generation of *A. thaliana* *pTCSn::GFP* × *pDR5v2::ntdTomato* Double Reporter Line:** A plasmid containing the molecular cassette *DR5v2::ntdTomato*<sup>[29]</sup> with kanamycin resistance (*pGIKDR5v2ntdTomato-tNOS-ntdTomato* plasmid) was kindly provided by C. Liao and D. Weijers. The plasmid was amplified and transformed into competent *Agrobacterium tumefaciens* cells with triple antibiotic resistance (rifampicin, tetracycline, and gentamycin). Successful transformants were selected, sequenced, and used to transform the *Arabidopsis* transgenic line *TCSn::GFP*<sup>[20]</sup> as described in Zhang et al.<sup>[56]</sup> The primers used were F<sub>1</sub>-DR5v2: GACCCTTCCTCTATATAAGG, R<sub>1</sub>-ntdT GCCCTCGATCTCGAACTCG (271 bp). Three independent transformations were carried out, i.e., three plants were dipped separately in the same *Agrobacterium* tube. Three plants from each kanamycin (50  $\mu\text{g mL}^{-1}$ ) selection plate that displayed double fluorescence (*TCSn::GFP* and *DR5v2::ntdTomato*) with the previously described expression

patterns<sup>[20,29]</sup> were transferred into soil. The presence of fluorescence was assessed in 5-day-old transformant roots using an epifluorescence microscope Leica DMi8. Homozygous lines for both reporter constructs were selected and used in further experiments.

**Confocal Imaging:** An AZ-C2 Nikon vertical macroconfocal system with a horizontally arranged AZ100 microscope was used to evaluate the real-time effect of OEIP-delivered iP on root development. To minimize drying of the sample, plates with *A. thaliana* seedlings were vertically mounted in a dark humidifying chamber equipped with an XYZ motorized stage (Prior Scientific fitted by Bergman-Labora) and diascopic white light and episcopic fluorescence light (Nikon). Each experiment began by setting up the optimized conditions for OEIP operation with a positive electrode placed in the OEIP reservoir with iP or [<sup>15</sup>N<sub>4</sub>]iP solution and a negative electrode in solid ½ MS medium in a Petri dish. The OEIP device was positioned precisely close to the root tip, LR, or LR primordia by employing a motor-drive micromanipulator MM-89 (Narishige, Japan). The first images of the control and OEIP-treated roots were acquired before applying the current (time 0 min). Confocal images were recorded with 2x AZ Plan Fluor 0.2 WD 45 mm or 5x AZ Plan Fluor 0.5 WD 15 mm DIC macro-objectives. The GFP signal was obtained by excitation at 488 nm, whereas the ntdTomato signal was acquired at 561 nm using the lasers of a C2+ confocal laser scanning system (Nikon). Images were recorded in Z-stack layers to capture the whole diameter of the root segment or LR. After taking the first image, a current of 25 nA was supplied to the electrodes to induce iP delivery. The roots were then imaged at different time-points for 8 h (root tips and LR) or after an overnight treatment (LR primordia).

**LC-MS/MS Quantification:** To optimize the iP delivery conditions, different cation delivery pumps, iP working concentrations and values of constant electrical current were tested by delivering iP into the liquid medium. The target media were collected after 2.5 h of iP delivery, then diluted 100x using 10% MeOH and analyzed with an LC-MS/MS system (1290 Infinity Binary LC System coupled to 6490 Triple Quad System with Jet Stream and Dual Ion Funnel technologies (Agilent Technologies)). 10  $\mu\text{L}$  of diluted media was injected onto a reversed-phase column (Acquity UPLC CSH C18, 130Å, 50×2.1 mm, 1.7  $\mu\text{m}$ ; Waters, Milford, MA, USA), iP was eluted during a 10 min linear gradient of 90:10 to 10:90 A:B, where ammonium formate (15 mM, pH 3.95) (A) and MeOH (B) served as the mobile phases, at a flow rate of 0.4 ml min<sup>-1</sup>. After every gradient run, the column was washed with 100% methanol (1.5 min) and equilibrated to the initial conditions (2.5 min). iP was introduced into the MS/MS system with the following settings: source gas temperature 200 °C; gas flow 16 L min<sup>-1</sup>; sheath gas temperature 375 °C; sheath gas flow 12 L min<sup>-1</sup>; nebulizer gas flow 35 psi; capillary voltage 2.7 kV. iP was detected using the multiple reaction monitoring (MRM) transition in the positive electrospray mode (ESI+) with MRM transition 204.1 > 136.1 when applying a collision energy of 13 eV. Chromatograms of detected iP were analyzed using MassHunter software (Agilent Technologies). The efficiency of iP transport was evaluated based on the size of MS peak areas after iP delivery under different delivery conditions. Conditions providing the highest peak area (i.e., highest transport efficiency) and adequate reproducibility of iP transport between technical replicates were selected as optimal.

To determine the OEIP-mediated delivery rate of iP under optimized conditions, the OEIP transport of iP was carried out in plastic microtubes filled with liquid ½ MS medium (100  $\mu\text{L}$ ). A constant current of 25 nA was applied to induce transport of iP into the media for 8 h. Every hour, the medium sample was collected and replaced by a microtube with a fresh medium. The collected medium samples were evaporated to dryness. Prior to purification, the samples were dissolved in formic acid (1 ml, 1 M). Isotopically labeled [<sup>15</sup>N<sub>4</sub>-purine]iP (0.25 pmol) synthesized as described in Buček et al.<sup>[57]</sup> was added as an internal standard to each sample and the samples were incubated for 30 min at 4 °C while shaking. Sample purification was achieved by solid-phase extraction using mixed-mode (strong cation exchange and reversed-phase) columns (Oasis MCX, 30 mg/1 ml; Waters), as described in Plačková et al.<sup>[58]</sup>

For iP and [ $^{15}\text{N}_4$ ]iP quantification in OEIP-treated roots, a 1 cm root segment from the proximity of the OEIP tip and corresponding 1 cm root segment of the control plant were collected after overnight treatment of LR primordia. The root segments were immediately frozen in liquid nitrogen and stored at  $-80^\circ\text{C}$  before analysis. Five root segments from different experiments were pooled and represented one biological sample for LC-MS/MS quantification. To quantify the endogenous levels of iP and [ $^{15}\text{N}_4$ ]iP together with their metabolites in the root segments, microextraction and StageTip purification methods published in Svačinová et al.<sup>[59]</sup> were used in slightly modified versions. Before purification, a mixture of internal deuterium ( $\text{d}_6$ )-labeled CK standards (0.25 pmol of CK free bases, ribosides and *N*-glucoside forms; 0.5 pmol of CK ribotides and *O*-glucosides; Olchemim Ltd) was added to each sample. After the sample purification, elution of the analytes from the StageTip microcolumns was achieved by adding ammonium hydroxide in 60% MeOH (50  $\mu\text{L}$ , 0.5 M). The samples were evaporated to dryness and redissolved by adding 5% MeOH (40  $\mu\text{L}$ ) before LC/MS/MS analysis.<sup>[59]</sup>

**Image Processing and Statistical Analysis:** Quantification of the GFP and ntdTomato fluorescent signals in the PR tip and LR was carried out using Fiji 2.1.1 software<sup>[60]</sup> and expressed as the corrected total cell fluorescence (CTCF) using the formula:  $\text{CTCF} = \text{integrated density} - (\text{area of selected cell} \times \text{mean fluorescence of three background readings})$ . All post-acquisition adjustments of images were carried out with the same settings for each experimental dataset using Fiji 2.1.1 software, Adobe Illustrator or Photoshop. Drawings were prepared with Adobe Illustrator. The fluorescent signal from the macroconfocal images was represented as a maximal intensity value of the Z-project from different focal plans. For quantification and statistics, GFP expression was examined in the stele of the PRs and LR and the fluorescent signal of ntdTomato was assessed in both stele and columella. Data were presented as means of  $\text{CTCF} \pm \text{SD}$  for  $n = 4$  (Figure 3, Figure S2),  $n = 7$  (Figure 5b) and  $n = 14$  (Figure 5c). Statistical analysis of the confocal data was achieved using two-tailed two-sided independent Student's *t*-tests in Excel (Microsoft Office) at  $\alpha = 5\%$ ,  $*P < 0.01$ ;  $**P < 0.01$ ;  $***P < 0.001$ , to compare the control treatments with iP application by OEIP. Further details of data normalization are given in each figure legend.

To investigate the effect of OEIP-delivered iP on PR tip development, the growth of treated and control root tips was reconstructed using *X* and *Y* coordinates acquired using the confocal microscopy software (NIS-Elements AR) as a difference in the coordinates at different time-points during 8 h of pumping and time 0 h ( $\Delta X [X_t - X_0]$ ,  $\Delta Y [Y_t - Y_0]$ ).

## Supporting Information

Supporting Information is available from the Wiley Online Library or from the author.

## Acknowledgements

The authors gratefully thank Dolf Weijers and Che-Yang Liao for sharing the plasmid to generate the *pDR5v2::Venus* marker line, and Rubén Casanova-Sáez for his help with the bacterial transformation. The authors are grateful to Ota Blahoušek for technical assistance with editing figures and to Ivan Petřík for his help with LC-MS/MS analyses. The authors also thank the Swedish Metabolomics Centre for the use of instrumentation. This work was supported by Knut and Alice Wallenberg (KAW) Foundation ShapeSystems project grant KAW 2012.0050. B. Parizkova was financially supported by the Ministry of Education, Youth and Sports of the Czech Republic through Mobility project no. CZ.02.2.69/0.0/0.0/16\_027/0008482 and the Kempe Foundation project no. JCK-1910. The work was additionally supported by the ERDF project "Plants as a tool for sustainable global development" (CZ.02.1.01/0.0/0.0/16\_019/0000827), project "Centre for Experimental Plant Biology" project no. CZ.02.1.01/0.0/0.0/16\_019/0000738 by the Ministry of Education,

Youth and Sports of the Czech Republic and by Czech Science Foundation (19-00973S). K.L. and I.A. were supported by grants from VR (Vetenskapsrådet), KAW and Vinnova.

## Conflict of Interest

The authors declare no conflict of interest.

## Data Availability Statement

The data that support the findings of this study are available from the corresponding author upon reasonable request.

## Keywords

*arabidopsis*, cytokinin, organic bioelectronics, hormone delivery, lateral root, root development, spatial resolution

Received: December 15, 2021

Revised: March 21, 2022

Published online:

- [1] T. Arbring Sjöström, M. Berggren, E. O. Gabrielsson, P. Janson, D. J. Poxson, M. Seitanidou, D. T. Simon, *Adv. Mater. Technol.* **2018**, 3, 1700360.
- [2] J. M. Leger, *Adv. Mater.* **2008**, 20, 837.
- [3] D. T. Simon, S. Kurup, K. C. Larsson, R. Hori, K. Tybrandt, M. Gojny, E. W. H. Jager, M. Berggren, B. Canlon, A. Richter-Dahlfors, *Nat. Mater.* **2009**, 8, 742.
- [4] A. Williamson, J. Rivnay, L. Kergoat, A. Jonsson, S. Inal, I. Uguz, M. Ferro, A. Ivanov, T. Arbring Sjöström, D. T. Simon, M. Berggren, G. G. Malliaras, C. Bernard, A. Williamson, A. Ivanov, C. Bernard, J. Rivnay, S. Inal, I. Uguz, M. Ferro, G. G. Malliaras, L. Kergoat, A. Jonsson, T. Arbring-Sjöström, D. T. Simon, M. Berggren, *Adv. Mater.* **2015**, 27, 3138.
- [5] K. Tybrandt, K. C. Larsson, S. Kurup, D. T. Simon, P. Kjäll, J. Isaksson, M. Sandberg, E. W. H. Jager, A. Richter-Dahlfors, M. Berggren, *Adv. Mater.* **2009**, 21, 4442.
- [6] A. Jonsson, T. A. Sjöström, K. Tybrandt, M. Berggren, D. T. Simon, *Sci. Adv.* **2016**, 2, e1601340.
- [7] D. T. Simon, K. C. Larsson, D. Nilsson, G. Burström, D. Galter, M. Berggren, A. Richter-Dahlfors, *Biosens. Bioelectron.* **2015**, 71, 359.
- [8] D. J. Poxson, M. Karady, R. Gabrielsson, A. Y. Alkattan, A. Gustavsson, S. M. Doyle, S. Robert, K. Ljung, M. Grebe, D. T. Simon, M. Berggren, *Proc. Natl. Acad. Sci. USA* **2017**, 114, 4597.
- [9] I. Bernacka-Wojcik, M. Huerta, K. Tybrandt, M. Karady, M. Y. Mulla, D. J. Poxson, E. O. Gabrielsson, K. Ljung, D. T. Simon, M. Berggren, E. Stavriniidou, *Small* **2019**, 15, <https://doi.org/10.1002/smll.201902189>.
- [10] G. R. Hicks, N. V. Raikhel, *Annu. Rev. Plant Biol.* **2012**, 63, 261.
- [11] K. Tybrandt, *Soft Matter* **2017**, 13, 8171.
- [12] D. J. Poxson, E. O. Gabrielsson, A. Bonisoli, U. Linderherd, T. Abrahamsson, I. Matthiesen, K. Tybrandt, M. Berggren, D. T. Simon, *ACS Appl. Mater. Interfaces* **2019**, 11, 14200.
- [13] H. Sakakibara, *Annu. Rev. Plant Biol.* **2006**, 57, 431.
- [14] S. Ha, R. Vankova, K. Yamaguchi-Shinozaki, K. Shinozaki, L. S. P. Tran, *Trends Plant Sci.* **2012**, 17, 172.
- [15] J. Banda, K. Bellande, D. von Wangenheim, T. Goh, S. Guyomarc'h, L. Laplace, M. J. Bennett, *Trends Plant Sci.* **2019**, 24, 826.



- [16] H. Jing, L. C. Strader, *Int. J. Mol. Sci.* **2019**, *20*, 486.
- [17] B. Péret, B. De Rybel, I. Casimiro, E. Benková, R. Swarup, L. Laplace, T. Beeckman, M. J. Bennett, *Trends Plant Sci.* **2009**, *14*, 399.
- [18] N. Svolacchia, E. Salvi, S. Sabatini, *Curr. Opin. Plant Biol.* **2020**, *57*, 133.
- [19] J. J. Kieber, G. E. Schaller, *Development* **2018**, *145*, 4.
- [20] E. Zürcher, D. Tavor-Deslex, D. Lituiev, K. Enkerli, P. T. Tarr, B. Müller, *Plant Physiol.* **2013**, *161*, 1066.
- [21] M. Seitanidou, K. Tybrandt, M. Berggren, D. T. Simon, *Lab Chip* **2019**, *19*, 1427.
- [22] M. Seitanidou, J. F. Franco-Gonzalez, T. A. Sjöström, I. Zozoulenko, M. Berggren, D. T. Simon, *J. Phys. Chem. B* **2017**, *121*, 7284.
- [23] L. M. Gonçalves, C. Batchelor-Mcauley, A. A. Barros, R. G. Compton, *J. Phys. Chem. C* **2010**, *114*, 14213.
- [24] A. M. Oliveira-Brett, L. A. da Silva, C. M. A. Brett, *Langmuir* **2002**, *18*, 2326.
- [25] T. I. Abdullin, I. I. Nikitina, O. V. Bondar, *Russ. J. Electrochem.* **2009**, *44*, 1345.
- [26] M. Adamowski, J. Friml, *Plant Cell* **2015**, *27*, 20.
- [27] J. Šimura, I. Antoniadis, J. Šíroká, D. Tarkowská, M. Strnad, K. Ljung, O. Novák, *Plant Physiol.* **2018**, *177*, 476.
- [28] I. Antoniadis, L. Plačková, B. Simonovik, K. Doležal, C. Turnbull, K. Ljung, O. Novák, *Plant Cell* **2015**, *27*, 1955.
- [29] C.-Y. Liao, W. Smet, G. Brunoud, S. Yoshida, T. Vernoux, D. Weijers, *Nat. Methods* **2015**, *12*, 207.
- [30] I. Antoniadis, O. Novák, Z. Gelová, A. Johnson, O. Plíhal, R. Šimerský, V. Mik, T. Vain, E. Mateo-Bonmatí, M. Karady, M. Pernisová, L. Plačková, K. Opasathian, J. Hejálko, S. Robert, J. Friml, K. Doležal, K. Ljung, C. Turnbull, *Nat. Commun.* **2020**, *11*, 4284.
- [31] K. Růžicka, M. Šimášková, J. Duclercq, J. Petrášek, E. Zažímalová, S. Simon, J. Friml, M. C. E. Van Montagu, E. Benková, *Proc. Natl. Acad. Sci. USA* **2009**, *106*, 4284.
- [32] B. Pařízková, M. Pernisová, O. Novák, *Int. J. Mol. Sci.* **2017**, *2736*.
- [33] Y. H. Su, Y. B. Liu, X. S. Zhang, *Mol. Plant* **2011**, *4*, 616.
- [34] R. Dello Ioio, K. Nakamura, L. Moubayidin, S. Perilli, M. Taniguchi, M. T. Morita, T. Aoyama, P. Costantino, S. Sabatini, *Science* **2008**, *322*, 1380.
- [35] R. Di Mambro, M. De Ruvo, E. Pacifici, E. Salvi, R. Sozzani, P. N. Benfey, W. Busch, O. Novak, K. Ljung, L. Di Paola, A. F. M. Marée, P. Costantino, V. A. Grieneisen, S. Sabatini, *Proc. Natl. Acad. Sci. USA* **2017**, *114*, E7641.
- [36] A. Nordström, *Ph.D. thesis*, Swedish University of Agricultural Sciences, Umeå **2004**.
- [37] M. Šmehilová, J. Dobrušková, O. Novák, T. Takáč, P. Galuszka, *Front. Plant Sci.* **2016**, *7*, <https://doi.org/10.3389/fpls.2016.01264>.
- [38] P. Hošek, K. Hoyerová, N. S. Kiran, P. I. Dobrev, L. Zahajská, R. Filepová, V. Motyka, K. Müller, M. Kamínek, *New Phytol.* **2020**, *225*, 2423.
- [39] K. Hoyerová, P. Hošek, *Front. Plant Sci.* **2020**, *11*, 5.
- [40] C. J. Liu, Y. Zhao, K. Zhang, *Front. Plant Sci.* **2019**, *10*, 613624.
- [41] W. Cajero Sánchez, B. García-Ponce, M. de la Paz Sánchez, E. R. Álvarez-Buylla, A. Garay-Arroyo, *Commun. Integr. Biol.* **2017**, *11*, e1395993.
- [42] R. Dello Ioio, F. S. Linhares, E. Scacchi, E. Casamitjana-Martinez, R. Heidstra, P. Costantino, S. Sabatini, *Curr. Biol.* **2007**, *17*, 678.
- [43] C. A. Auer, *J. Plant Growth Regul.* **1996**, *15*, 201.
- [44] T. Werner, V. Motyka, M. Strnad, T. Schmülling, *Proc. Natl. Acad. Sci. USA* **2001**, *98*, 10487.
- [45] G. Bertell, L. Eliasson, *Physiol. Plant.* **1992**, *84*, 255.
- [46] X. Li, X. Mo, H. Shou, P. Wu, *Plant Cell Physiol.* **2006**, *47*, 1112.
- [47] L. Chang, E. Ramireddy, T. Schmülling, *J. Exp. Bot.* **2013**, *64*, 5021.
- [48] S. Ubeda-Tomás, F. Federici, I. Casimiro, G. T. S. Beemster, R. Bhalerao, R. Swarup, P. Doerner, J. Haseloff, M. J. Bennett, *Curr. Biol.* **2009**, *19*, 1194.
- [49] T. Beeckman, S. Burssens, D. Inze, *J. Exp. Bot.* **2001**, *52*, 403.
- [50] P. Marhavý, A. Bielach, L. Abas, A. Abuzeineh, J. Duclercq, H. Tanaka, M. Pařezová, J. Petrášek, J. Friml, J. Kleine-Vehn, E. Benková, *Dev. Cell* **2011**, *21*, 796.
- [51] A. Bielach, K. Rina Podlešáková, P. Marhavý, J. Duclercq, C. Cuesta, B. Müller, W. Grunewald, P. Tarkowski, E. Benková, *Plant Cell* **2012**, *24*, 3967.
- [52] G. Márquez, M. V. Alarcón, J. Salguero, *J. Plant Growth Regul.* **2019**, *38*, 83.
- [53] E. O. Gabrielsson, Y. H. Jung, J. H. Han, D. J. Joe, D. T. Simon, K. J. Lee, M. Berggren, *Adv. Mater. Technol.* **2021**, *6*, 2100526.
- [54] M. Seitanidou, R. Blomgran, G. Pushpamithran, M. Berggren, D. T. Simon, *Adv. Healthcare Mater.* **2019**, *8*, 1900813.
- [55] J. Courtois, M. Szumski, E. Byström, A. Iwasiewicz, A. Shchukarev, K. Irgum, *J. Sep. Sci.* **2006**, *29*, 14.
- [56] X. Zhang, R. Henriques, S.-S. Lin, Q.-W. Niu, N.-H. Chua, *Nat. Protoc.* **2006**, *1*, 641.
- [57] J. Buček, M. Zatloukal, L. Havlíček, L. Plíhalová, T. Pospíšil, O. Novák, K. Doležal, M. Strnad, *R. Soc. Open Sci.* **2018**, *5*, 181322.
- [58] L. Plačková, J. Oklestkova, K. Pospíšková, K. Poláková, J. Buček, J. Stýskala, M. Zatloukal, I. Šafařík, R. Zbořil, M. Strnad, K. Doležal, O. Novák, *Plant J.* **2017**, *89*, 1065.
- [59] J. Svačinová, O. Novák, L. Plačková, R. Lenobel, J. Holík, M. Strnad, K. Doležal, *Plant Methods* **2012**, *8*, 17.
- [60] J. Schindelin, I. Arganda-Carreras, E. Frise, V. Kaynig, M. Longair, T. Pietzsch, S. Preibisch, C. Rueden, S. Saalfeld, B. Schmid, J. Y. Tinevez, D. J. White, V. Hartenstein, K. Eliceiri, P. Tomancak, A. Cardona, *Nat. Methods* **2012**, *9*, 676.